

Unraveling Supported Lipid Bilayer Formation Kinetics: Osmotic Effects

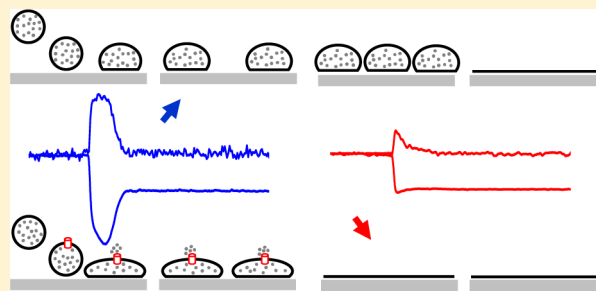
Nicole Hain,^{†,‡,§} Marta Gallego,[†] and Ilya Reviakine^{*,†}

[†]CIC biomaGUNE, Paseo Miramón 182, San Sebastián 20009, Spain

[‡]Institute of Physical Chemistry, Clausthal University of Technology, Arnold-Sommerfeld-Str. 4, D-38678 Clausthal-Zellerfeld, Germany

Supporting Information

ABSTRACT: Solid-supported lipid bilayers are used as cell membrane models and form the basis of biomimetic and biosensor platforms. The mechanism of their formation from adsorbed liposomes is not well-understood. Using membrane-permeable solute glycerol, impermeable solutes sucrose and dextran, and a pore forming peptide melittin, we studied experimentally how osmotic effects affect the kinetics of the adsorbed liposome-to-bilayer transition. We find that its rate is enhanced if adsorbed liposomes are made permeable but is not significantly retarded by impermeable solutes. The results are explained in terms of adsorbed liposome deformation and formation of transmembrane pores.



INTRODUCTION

The behavior of liposomes adsorbed on surfaces of inorganic materials is complex and, despite nearly 20 years of research, remains poorly understood.^{1–10} On the one hand, it is governed by the sign (attractive or repulsive) and the strength of the lipid–surface interactions. On the other hand, there are kinetic effects that control adsorbed liposome stability. Ultimately, the fate of the adsorbed liposomes is determined by a balance between these two factors. How they are related to the properties of the surface, or to the properties of the liposomes, is not clear.

Sufficiently strong attractive interactions arise, for example, in the case of positively charged liposomes on negatively charged substrates.^{6,9,11,12} They result in the rupture of individual adsorbed liposomes into single bilayer patches. A confluent bilayer (supported lipid bilayer or SLB^{13,14}) eventually forms on the surface as liposomes continue to adsorb and rupture. If the attraction is too weak, adsorbed liposome layers (so-called supported vesicular layers or SVLs^{1–4,9,15,16}) may remain on the surface virtually indefinitely, separated from the bilayer by an energy barrier. At intermediate attraction strength, this energy barrier may be overcome. In that case, adsorbed liposomes rupture collectively in a process called “neighbor-induced decomposition” that also leads to the formation of an SLB.^{3,15} It is thought to be initiated by clusters of two or more adsorbed liposomes in contact with each other and may involve fusion of adjacent liposomes.^{4,17}

In numerous previous studies, lipid–surface interactions were varied to examine their effect on the SLB formation kinetics. This was achieved, for example, by varying lipid charge,^{9,11,12} surface charge,^{2,18} or ionic strength.^{5,19–21} An

aspect that has been almost entirely neglected pertains to the deformation of adsorbed liposomes upon adsorption and the associated osmotic effects.

Liposomes deform upon adsorption.^{17,22} This is well-known in the case of giant liposomes, but recently it was also demonstrated for liposomes with sizes in the range of tens of nanometers.^{23,24} In the presence of osmotically active substances, the change in the internal volume associated with the deformation leads to an osmotic pressure buildup. In this study, we examine how this osmotic pressure buildup affects the rate of supported bilayer formation. This was achieved by following SLB formation from liposomes prepared under four sets of conditions. In one case, liposomes were prepared in buffers containing various concentrations of glycerol. In another case, they were prepared in buffers containing various concentrations of sucrose. In the third case liposomes were prepared in a standard aqueous buffer (without sucrose or glycerol) and mixed with a pore-forming peptide melittin.^{25,26} In the fourth case, liposomes were prepared in a buffer containing 5 kDa dextran and then mixed with melittin. In all cases, liposomes were prepared under isotonic conditions.

The rationale for selecting these four sets of conditions is as follows. Glycerol and melittin are expected to prevent the osmotic pressure from building up in the adsorbing liposomes. Melittin does so by allowing osmotically active substances to escape from the interior of the liposomes, while glycerol itself is a permeable solute.^{27–29} However, glycerol affects parameters

Received: October 23, 2012

Revised: January 8, 2013

such as buffer viscosity, which is expected to control liposome rupture rate.³⁰ Therefore, we used sucrose-containing buffers of identical viscosity as a control. Similarly, dextran that is too large to pass through the melittin-formed pores was used as a control to rule out possible effects of melittin on lipid bilayer stability. Finally, both sucrose and glycerol may affect lipid–surface interactions. By comparing the effects of the permeable solute/impermeable solute (glycerol/sucrose) pair on the SLB formation kinetics with that of melittin/dextran, we are able to rule out the possibility that changes in lipid–surface interactions or liposome stability are responsible for the changes in the SLB formation rates and conclude that the effects we observe are indeed related to permeability and therefore to osmotic pressure build up in the adsorbing liposomes.

We would like to note that previously Reimhult et al. used salt solutions of different concentrations inside and outside to osmotically stress liposomes prior to adsorption; this had the effect of speeding up SLB formation.⁵ However, lipid–surface interactions also depend on the ionic strength.^{19–21,31,32} Therefore, the effect of a salt gradient on the SLB formation kinetics results from at least two contributions: changes in the lipid–surface interactions and the osmotic effects. Furthermore, electrostatic gradients destabilize the membrane (independently of the direction of the gradient). Our approach allows us to avoid these complications.

MATERIALS AND METHODS

Materials. Chemicals used ($\geq 99.0\%$ purity) and analytical standard dextran (MW 5220 Da) were purchased from Sigma-Aldrich (Madrid, Spain), except for NaOH which was purchased from Scharlab (Barcelona, Spain).

Powdered L- α -phosphatidylcholine 95% (egg yolk, EggPC) and 1,2-doleoyl-*sn*-glycero-3-phosphocholine (DOPC, >99%) were purchased from Avanti Polar Lipids, Inc. (Alabaster, AL), and stored at $-20\text{ }^{\circ}\text{C}$ until used. Lipid stock solutions were prepared by dissolving the lipid powder in chloroform stabilized with 0.5–1.0% ethanol in a 2 mL clear-glass vial with a preassembled screw top with a PTFE linear (Sigma-Aldrich, Madrid, Spain). Lipid stock solutions were stored at $-20\text{ }^{\circ}\text{C}$ until used, but for no longer than 2 months. Lipid concentration in the stock solutions was checked by phosphorus determination following the protocol from Avanti Polar Lipids (published on their Web site).

The standard buffer used throughout this study was 10 mM HEPES, 150 mM NaCl, and 2 mM $\text{CaCl}_2 \cdot 6\text{H}_2\text{O}$, pH 7.4. Glycerol, sucrose, and dextran-containing buffers were made by mixing this standard buffer with appropriate volumes of glycerol (5%, 10%, 15%, 20%, 30%, or 40%, v/v) or dissolving appropriate amounts of sucrose (16.9% or 31.7% w/v) or dextran (final concentration of dextran was 10 μM). Note that the viscosity of 16.9% sucrose-containing buffer solution is equivalent to that of the 20% glycerol solution, and the viscosity of the 31.7% sucrose solution is equivalent to that of the 40% glycerol solution. Buffers were filtered through a 0.2 μm pore-diameter sterile syringe filters (Fisher Scientific, Madrid, Spain) and degassed for 30 min in a water bath sonicator with degas function (Fisher Scientific, Madrid, Spain) immediately before use.

Water used in this study was purified in a Water Purification System Diamond UV (Branstead International, Dubuque, IA) that produces particle-free nanopure water with less than 1 ppb total organic carbon and 18.2 $\text{M}\Omega \cdot \text{cm}$ resistivity.

Nitrogen and high purity argon gases were purchased from Air Liquid S.L. (Madrid, Spain). A 0.2 μm sterile filter (Fisher Scientific, Madrid, Spain) was attached to the nitrogen gun (Skan AG, Basel, Switzerland) in order to obtain a particle-free flow.

Methods. *Liposome Preparation and Characterization.* Multilamellar vesicles (MLVs) were prepared from EggPC or DOPC as described in ref 4. Briefly, the desired amount of the lipid stock

solution was deposited into a round-bottom glass test tube. Chloroform was evaporated under a stream of argon. The resulting thin film was further dried at room temperature under vacuum generated by an oil-free diaphragm pump for 1 h. The dried lipid film was resuspended in an appropriate buffer (either free from additives or containing one of glycerol, sucrose, or dextran at appropriate concentrations) by vortexing to form MLVs.

Sonicated unilamellar vesicles (SUVs) were prepared by sonication of the MLV suspension at $0\text{ }^{\circ}\text{C}$ under nitrogen atmosphere for 1 h³³ using a 450 Branson Sonicator (Branson Ultrasonic, Danbury, CT) set at 30% duty cycle and at an output power of 3. SUVs were purified by centrifugation at 6500g at $4\text{ }^{\circ}\text{C}$ for 3 h in a Sigma 3K30 centrifuge (Sigma Centrifuges, Shropshire, U.K.) under an argon atmosphere. SUVs were not separated from the nonencapsulated molecules in order to avoid osmotic stress on the vesicles. Vesicle suspensions were analyzed by dynamic light scattering using a Zetasizer Nano series instrument (Malvern, Worcestershire, U.K.). The results are shown in Table S1 of the Supporting Information.

Quartz Crystal Microbalance (QCM) Measurements. Five MHz SiO_2 -coated quartz crystals were purchased from Biolin Scientific AB (Solna, Sweden). Crystals were cleaned in 2% sodium dodecyl sulfate solution for 30 min, then thoroughly rinsed with nanopure water, dried under a flow of nitrogen, and treated for 30 min in a UV–ozone cleaner (BioForce Nanosciences, Ames, IA). The UV–ozone cleaner was preheated for 30 min before use. After cleaning, crystals were used immediately.

Clean crystals were mounted in the Q-Sense flow modules. QCM was performed using a hybrid QCM system described elsewhere.³⁴ Briefly, an E5100A network analyzer (Agilent; Madrid, Spain) controlled by the QTZ software (Resonant Probes GmbH, Goslar, Germany) was used to passively acquire the impedance spectrum of the crystal at several overtones (between 15 and 84 MHz) and fitted to obtain the resonance frequency f_n and bandwidth Γ_n on each overtone. Experiments were performed under stagnant conditions at $20 \pm 1\text{ }^{\circ}\text{C}$. The temperature was controlled with a water circulator (Analogue model 912, Polyscience, Niles, IL). Liposome concentration used in QCM experiments was always 0.05 mg/mL. For convenience, the results are reported in terms of the dissipation, $D_n = 2\Gamma_n/f_n$, rather than the bandwidth. The data obtained on the fifth overtone are presented in the figures.

Before and after each measurement, flow modules were disassembled and cleaned by sonication in Cobas Integra Cleaner (Roche Diagnostics S.L., Barcelona, Spain) for 15 min followed by sonication in three changes of nanopure water, 10 min each, and dried under a stream of nitrogen. The assembly of the modules and mounting of the crystals were done in a laminar flow hood (Airstream, Esco GB Ltd., Wiltshire, U.K.).

Atomic Force Microscopy (AFM) Imaging. AFM images were acquired in tapping mode on a Multimode atomic force microscope connected to a Nanoscope V controller equipped with a “J” (125 μm) scanner and a fluid cell with oxide-sharpened silicon nitride cantilevers mounted on 120 μm triangular cantilevers with nominal spring constants of 0.24 N/m. All the components were from Bruker Nano Surfaces Division (Santa Barbara, CA).

$1.1 \times 1.1\text{ cm}^2$ pieces of silicon wafers (University Wafer, South Boston, MA) were cleaned for 10 min in 1:1:1.5 mixture of $\text{NH}_4\text{OH}:\text{H}_2\text{O}_2:\text{H}_2\text{O}$ at $55\text{ }^{\circ}\text{C}$, rinsed with nanopure water, cleaned in 1:1:1.5 mixture of $\text{HCl}:\text{H}_2\text{O}_2:\text{H}_2\text{O}$ at $55\text{ }^{\circ}\text{C}$ for 10 min, rinsed with nanopure water, and immediately glued to the BYTAC adhesive tape-covered metal discs used for mounting samples in the AFM with double-sided tape. This sample assembly procedure is based on that used by Muller et al.³⁵ The sample was mounted on the AFM scanner, and the tapping mode fluid cell with an S-shaped silicon O-ring was assembled on top. The cell was filled with the relevant buffer, and the microscope was allowed to thermally equilibrate for at least 30 min. The bare surface was imaged to ascertain its cleanliness.

If the surface was found to be free of contamination, 2 mL of sonicated liposome solution containing $4 \times 10^{-3}\text{ mg/mL}$ lipid was injected into the fluid cell. Liposomes were allowed to adsorb for 30 min, and the surface was imaged. The procedure of injection of 1 mL

of liposome solution, equilibration, and imaging was repeated until the surface was covered with a bilayer. Images were plane-fitted and flattened as required, exported into AdobePhotoshop, where they were resized and brightness and contrast were adjusted.

RESULTS AND DISCUSSION

To examine SLB formation kinetics, we use quartz crystal microbalance (QCM or QCM-D, see ref 36 for a recent review) because this technique can distinguish between adsorbed liposomes and bilayers.^{3,6,9,12,15} QCM measures the resonance frequency of the quartz crystal f and the dissipation $D = 2\Gamma/f$, where Γ is the half-band half-width of the resonance. Changes in the resonance frequency relative to those of the bare crystal, Δf , as material accumulates at the surface are related to the average thickness of the layer of material on the surface. Dissipation arises from adsorbed liposomes only—neither a confluent bilayer nor bilayer patches dissipate.^{3,6,9,12,15} Therefore, adsorption of liposomes to the surface causes a decrease in the frequency and an increase in the dissipation (Figure 1).

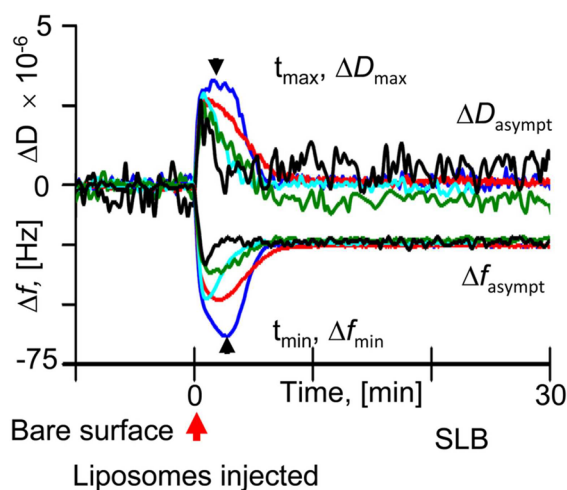


Figure 1. SLB formation kinetics measured with QCM. Frequency and dissipation shifts, Δf and ΔD , plotted as a function of time, obtained with egg phosphatidyl choline liposomes in glycerol-containing buffers of various compositions on SiO_2 -coated QCM crystals. Liposome injection is at time zero. Adsorption of liposomes to the surface causes a decrease in the frequency and an increase in the dissipation, while their rupture causes an increase in frequency and a decrease in the dissipation. The dissipation returns to zero ($\Delta D_{\text{asympt}} \sim 0$) and the frequency to a value of $\Delta f_{\text{asympt}} \sim -25$ Hz, corresponding to SLB formation. Blue: 0% glycerol; red: 10% glycerol (v/v); cyan: 15%; olive: 20%; black: 40% in 10 mM HEPES, 2 mM CaCl_2 , 150 mM NaCl buffer. The level of noise increases with the glycerol content due to an increase in the viscous damping of the resonance associated with the increase in the buffer viscosity. The parameters extracted from these measurements, t_{min} , Δf_{min} , t_{max} , ΔD_{max} , Δf_{asympt} and ΔD_{asympt} are indicated with black arrowheads.

Rupture of liposomes leads to an increase in the frequency and a decrease in the dissipation (Figure 1). The overall trajectory of the QCM signals depends on the relative rates of the two processes: liposome adsorption and liposome rupture. In the case of neighbor-induced decomposition, rupture rate increases with surface coverage because several liposomes need to be in contact to initiate rupture, and this becomes more likely as coverage increases. When the two rates are comparable, extrema in frequency and dissipation are observed. They were first reported by Keller and Kasemo³ and are visible in the Δf

and ΔD vs time curves shown in Figure 1. Their magnitudes, Δf_{min} and ΔD_{max} and the time it takes to reach them (t_{min} and t_{max} respectively), diminish with increasing interaction strength¹¹ as the rate of liposome rupture increases and vanish entirely when the attraction is strong enough for liposomes to rupture directly upon adsorption^{6,9,12}—in other words, when the rate of liposome rupture exceeds that of liposome adsorption. Because these parameters are sensitive to the liposome rupture rate, we use them to monitor SLB formation kinetics. (t_{min} , Δf_{min}) and (t_{max} , ΔD_{max}) were extracted from the curves such as those shown in Figure 1. Their values are plotted in Figures 2 and 3 as a function of the different experimental variables (glycerol or sucrose contents in the buffer in Figure 2, melittin:lipid ratio in Figure 3).

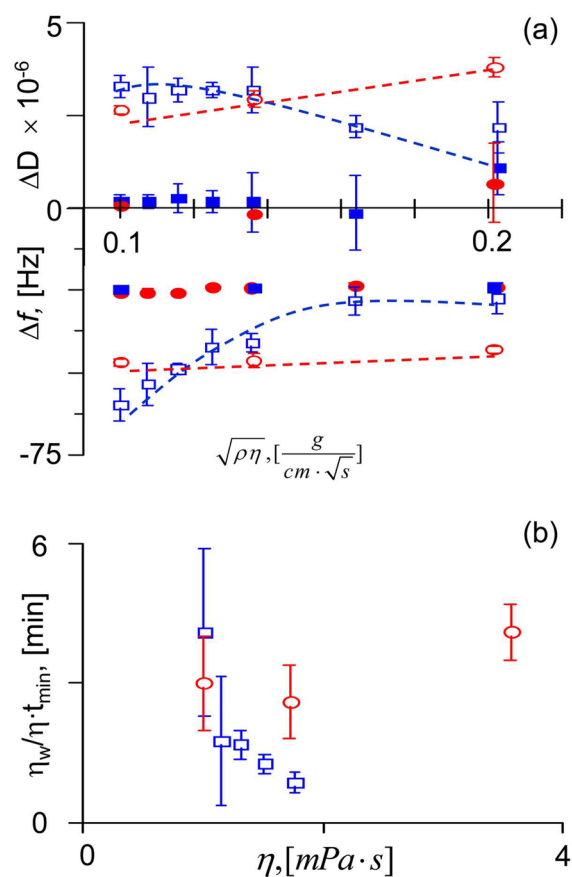


Figure 2. Effect of solute permeability on the SLB formation rate. (a) Plots of ΔD_{max} , ΔD_{asympt} and Δf_{asympt} , Δf_{min} extracted from the measurements such as the one shown in Figure 1. Filled symbols: asymptotic shifts. Open symbols: extrema. Measurements done in glycerol-containing buffers: blue squares. Measurements done in sucrose-containing buffers: red circles. The shifts are plotted as a function of the square root of the buffer viscosity–density product to rule out contributions of buffer viscosity and density to the results. Mean \pm std dev of at least three experiments are shown. Dashed lines are guides to eye. (b) The time it takes to reach the minimum in frequency, t_{min} , scaled by the ratio of viscosities (viscosity of water/viscosity of buffer of a particular composition) to account for the difference in transport conditions, is plotted against the solution viscosity for the experiments done in glycerol (blue squares) and in sucrose (red circles). It was no longer possible to accurately determine t_{min} in buffers containing 30% and 40% glycerol. Plots of t_{max} , the time it takes to reach the maximum in dissipation, show similar trends (not shown).

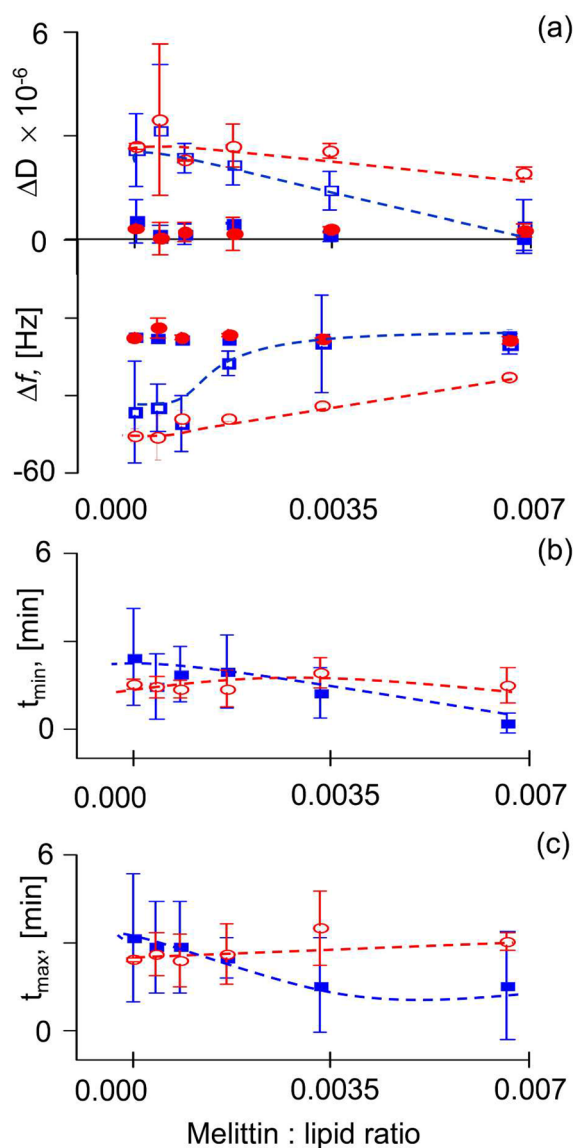


Figure 3. Effect of melittin-induced pores on the SLB formation kinetics. (a) Plots of ΔD_{\max} , ΔD_{asympt} , and Δf_{asympt} , Δf_{\min} obtained from QCM experiments performed with liposomes prepared in the presence of melittin (blue squares) and melittin + 5 kDa dextran (red circles) as a function of the melittin:lipid ratio in the liposomes. Filled symbols: asymptotic shifts. Open symbols: extrema. (b, c) Plots of t_{\min} and t_{\max} respectively. The color code is the same as in (a): melittin, blue squares; melittin + 5 kDa dextran, red circles. Lines are guides to eye. Average \pm std dev of at least three measurements are shown.

In this study, we used liposomes composed of fluid-phase phosphatidylcholines (PCs) prepared by sonication in 10 mM HEPES, 150 mM NaCl, and 2 mM CaCl_2 , pH 7.4 buffer, containing either 0–40 vol % of glycerol, 0–32 wt % of sucrose, or 10 μM 5 kDa dextran. No effect of glycerol or sucrose on the liposome size was observed (see Table S1 in the Supporting Information). This is consistent with previously published results.^{37–39} Addition of melittin to the liposomes lead to an increase in their size, as expected.²⁵ QCM experiments were performed with melittin/lipid molar ratios <0.007 to minimize this effect.

Bilayers were formed from these liposomes under all of the conditions used in this study. Indeed, at the end of each experiment, we found frequency and bandwidth shifts of ~ -25

Hz and ~ 0 , respectively—typical of an SLB.³ An independent confirmation of bilayer formation in the presence of glycerol and sucrose was also obtained by atomic force microscopy (see Figure S2 in the Supporting Information).

Importantly, the peak in frequency, Δf_{\min} , was found to diminish with increasing glycerol content and vanished altogether by $\sim 30\%$ glycerol (Figures 1 and 2a); the peak in dissipation ΔD_{\max} diminished but did not disappear completely. The time it takes to reach the minimum in frequency, t_{\min} (Figure 2b), decreased with glycerol content. The values of t_{\min} plotted in Figure 2b are normalized to account for the changes in the transport rate due to the changes in the solution viscosity. Therefore, the observed reduction in t_{\min} indicates that the rate of liposome rupture increases with the glycerol content. From t_{\min} values, one can estimate the absolute values of the liposome surface coverage at the steady state (when the rate of rupture and rate of adsorption balance each other) using the equation for adsorption from stagnant solution $G(t) = 2c(tkT/(6\pi^2\eta R))^{1/2}$,⁴⁰ where G is the surface coverage, t is time, η is the solution viscosity, and R is the liposome radius. Substituting 4 min for t (the t_{\min} value in the absence of glycerol), 40 nm for the vesicle radius, a lipid concentration of 0.05 mg/mL (converted into liposome concentration via the area per lipid of 0.72 nm²), and the appropriate value for solution viscosity, one obtains the coverage of $\sim 13 \pm 3\%$ at t_{\min} . This changes to $\sim 6 \pm 1.6\%$ for t_{\min} of 1.5 min observed in the 20% glycerol solution ($t_{\min}\eta_w/\eta = 0.9$). (Note that surface coverage here is expressed in terms of the undeformed liposomes occupying an area πR^2 on the surface.) Essentially, this indicates that the amount of material on the surface at the steady state decreases with increasing glycerol content. Observed changes in Δf_{\min} and ΔD_{\max} are consistent with this.

Impermeable solute sucrose had a limited effect on the bilayer formation, slowing it down somewhat (relative to the situation in the absence of sucrose): there is an increase in ΔD_{\max} , no change in Δf_{\min} (Figure 2a), and an increase in t_{\min} (Figure 2b).

Melittin is a 26-amino acid amphipathic peptide. It is the principal component of bee venom.²⁶ When incorporated into lipid bilayers, melittin is thought to form pores. Pore size depends on the melittin-to-lipid ratio.²⁵ When we performed SLB formation experiments with melittin-containing liposomes (Figure 3), we found that melittin had an effect similar to that of glycerol: the magnitude of the extrema and the time it took to reach the extrema diminished with increasing melittin:lipid ratio (blue symbols in Figure 3).

To verify that the observed effect of melittin was related to permeability, we performed the same set of experiments in the presence of 5 kDa dextran. At the melittin:lipid ratios we use, the pores formed by melittin are too small for the dextran of this size to penetrate through them.²⁵ Indeed, dextran is seen to diminish the effect of melittin (red symbols in Figure 3).

In summary, we observe that the rate of adsorbed liposome rupture is significantly enhanced if adsorbing liposomes are made permeable in one way or another but is diminished, though not to the same extent, by inclusion of impermeable solutes. Our interpretation of these results is schematically illustrated in Figure 4 and proceeds as follows. Liposome deformation leads to a reduction of the internal volume as water leaves the liposomes. In the presence of osmotically active substances (including common buffers and salts) this results in an osmotic pressure that limits the deformation (Figure 4a). This effect can be illustrated by the following back-

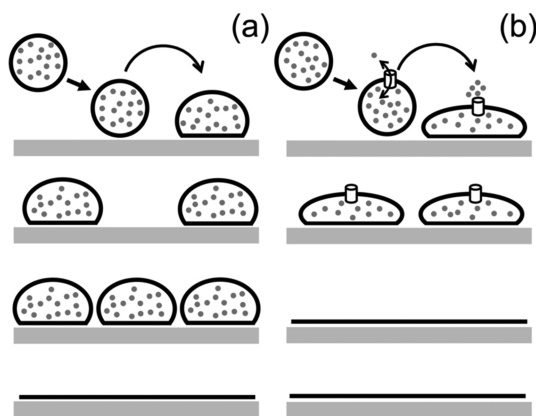


Figure 4. Schematic illustration of the effect liposome permeability has on the SLB formation rate. Permeability (by virtue of pores or a permeable solute) allows greater extent of deformation upon adsorption. This increases the number of liposome–liposome contacts needed to initiate SLB formation and reduces the number of liposomes on the surface at the steady state. (a) Liposomes adsorbing in the presence of osmotically active substances. (b) Permeable liposomes (prepared in the presence of melittin or glycerol).

of-the-envelope calculation. The shape of an adsorbed liposome results from a balance between the adhesion energy, curvature energy, membrane tension, and osmotic pressure. On the one hand, lipid–surface attraction causes adhesion. The system gains energy by maximizing the liposome–surface contact area. On the other hand, this results in liposome deformation. Associated with the deformation is the cost of changes in membrane curvature (bending), the cost of changes in the liposome area (membrane tension), and, in the presence of osmotically active substances, the osmotic pressure that results from the changes in liposome volume. Let us take a deformed liposome with the shape illustrated in Figure 1 in Seifert and Lipowsky.²² It is calculated at a reduced potential $w = WR^2/\kappa = 10.2$ (where W is the adhesion energy, R is the liposome radius, and κ is the bilayer bending modulus), at a constant area $A = 4\pi R^2$, and a pressure of zero (no osmotically active substances present). In other words, for this particular case, there are only two contributions—adhesion and bending—and they balance each other. This allows us to straightforwardly calculate W from w . For the liposome radius of ~ 40 nm and bilayer bending modulus of $\sim 1 \times 10^{-19}$ J, W is ~ 0.6 mJ/m², and the energy gain due to adhesion Wa , where a is the liposome–surface contact area, is $\sim 4 \times 10^{-18}$ J. To calculate a , we approximated adsorbed liposome shape by that of a spherical cap. The area of a spherical cap is equal to the total area of the liposome, $A = \pi r^2 + \pi(h^2 + r^2)$, where r is the radius of the base and h is the height of the cap. Rearranging gives us the area of the base: $a = A/2((h/2R)^2 - 1)$. The ratio $h/(2R)$ can be read directly from the Y -axis in Figure 1 of ref 22. Membrane tension, which scales as W/k ,¹⁷ where $k \sim 240$ mJ/m² (see ref 41) is the area compressibility modulus of the bilayer, for this value of W is negligible, justifying the constant area assumption made above.

On the other hand, the work $p\Delta V$, where p is the osmotic pressure, associated with the corresponding change in the liposome volume, is significantly greater: $\sim 6 \times 10^{-17}$ J. Here, again, the volume of a spherical cap $V = \pi h^2/3(3R - h)$ was used to calculate ΔV , and a buffer osmolarity of 300 mOsm/L was used to calculate $p = RT\Delta c$, where Δc is the change in the solute concentration inside the adsorbing liposome, T is temperature, and R is the universal gas constant.

This result means that to achieve the level of deformation corresponding to $w = 10.2$ in the absence of the osmotic pressure, W would have to be more than 10 times higher (8.8 mJ/m²) in its presence. This adhesion potential is sufficiently high to rupture the membrane. Even for the least deformed shape shown in that figure (corresponding to $w = 2.9$), the osmotic contribution is of the same order of magnitude as the bending contribution (1.3×10^{-19} J vs 3.2×10^{-19} J), and its effect in determining the adsorbed liposome shape (extent of deformation) is therefore significant.

Tension that builds up in the bilayer of the adsorbing liposomes as a result of the osmotic pressure or as a result of adhesion may be released via the formation of transient pores that do not lead to liposome rupture but allow partial or complete equilibration of internal solution with the outside. Such transient pores and equilibration processes have indeed been inferred or directly observed: in nanometer-sized adsorbed liposomes^{42–44} as well as in osmotically stressed extruded⁴⁵ and giant²⁸ liposomes in solution. Furthermore, lipid bilayers can withstand considerable osmotic gradients without rupturing or forming pores virtually indefinitely: e.g., a 40 nm liposome can withstand a gradient of up to ~ 800 mOsm/L.⁴⁵ It is for these reasons sucrose had a limited effect on the SLB formation rate in our experiments.

Glycerol, a permeable solute,^{27–29} will be expelled preferentially (relative to water), allowing for a greater deformation (Figure 4b) because the solubility of NaCl in glycerol is 83 g/kg, compared to 360 g/kg in water,⁴⁶ and because it is larger than water. Differential transport of water and glycerol across liposome membranes has been observed in experiments where giant liposomes prepared in sucrose solutions were transferred into glycerol-containing sucrose-free buffers.²⁸ These liposomes were observed to burst, in a cyclical fashion, indicating that the influx of glycerol into the liposomes was not balanced by the outward flux of water. Melittin-induced pores in the membrane have a similar effect because they allow the internal solution to be equilibrated with the outside (Figure 4b). 5 kDa dextran diminishes this effect because it cannot pass through the pores. On the other hand, it does not eliminate the effect of melittin completely because there are other osmotically active substances present inside the liposomes that are smaller and can equilibrate through the melittin-formed pores.

In the case of neighbor-induced rupture pathway, SLB formation is thought to be initiated by contact between two or more adsorbing liposomes. Because the area occupied by the liposomes on the surface increases with their deformation, such events become more likely. Therefore, the rate of liposome rupture increases with increasing deformation, and fewer liposomes need to adsorb to the surface to reach the steady state. This explains the observed trends in t_{\min} , t_{\max} , Δf_{\min} , and ΔD_{\max} .

We note that the effect of permeability is merely kinetic. In other words, we do not observe a change from the neighbor-induced decomposition pathway to an individual rupture pathway by altering permeability—either with glycerol or with melittin. This can be inferred from the nonzero dissipation observed with QCM (Figures 2 and 3), which means that adsorbed liposomes are still present on the surface during the SLB formation. The presence of adsorbed liposomes is also supported by the AFM images (Figure S1 in the Supporting Information).

CONCLUSIONS

We have shown that SLB formation rate is linked to adsorbed liposome deformation, which in this system is controlled by osmotic effects resulting from the volume changes due to the adsorbed liposome deformation. This effect has been neglected in previous studies of supported lipid bilayer formation kinetics. Its understanding will undoubtedly lead to a revision of the current models of the SLB formation process.

ASSOCIATED CONTENT

Supporting Information

Details of liposome characterization and AFM images of supported bilayer formation in glycerol- and sucrose-containing buffers. This material is available free of charge via the Internet at <http://pubs.acs.org>.

AUTHOR INFORMATION

Corresponding Author

*E-mail: IReviakine@cicbiomagune.es.

Present Address

[§]Institute of Physical Chemistry I, University of Siegen, AR-F0103, Adolf-Reichwein-Str. 2, 57076 Siegen, Germany.

Notes

The authors declare no competing financial interest.

ACKNOWLEDGMENTS

We acknowledge the funding from the Department of Industry of the Basque Government (program ETORTEK) and from the Spanish Ministry of Science and Innovation (MICINN, ref CTQ2009-11245) to I.R. N.H. was supported by an ERASMUS grant through the Project MixIt.

REFERENCES

- (1) Nollert, P.; Kiefer, H.; Jahnig, F. Lipid vesicle adsorption versus formation of planar bilayers on solid-surfaces. *Biophys. J.* **1995**, *69* (4), 1447–1455.
- (2) Cremer, P. S.; Boxer, S. G. Formation and spreading of lipid bilayers on planar glass supports. *J. Phys. Chem. B* **1999**, *103* (13), 2554–2559.
- (3) Keller, C. A.; Kasemo, B. Surface specific kinetics of lipid vesicle adsorption measured with a quartz crystal microbalance. *Biophys. J.* **1998**, *75* (3), 1397–1402.
- (4) Reviakine, I.; Brisson, A. Formation of supported phospholipid bilayers from unilamellar vesicles investigated by atomic force microscopy. *Langmuir* **2000**, *16* (4), 1806–1815.
- (5) Reimhult, E.; Hook, F.; Kasemo, B. Intact vesicle adsorption and supported biomembrane formation from vesicles in solution: Influence of surface chemistry, vesicle size, temperature, and osmotic pressure. *Langmuir* **2003**, *19* (5), 1681–1691.
- (6) Edvardsson, M.; Svedhem, S.; Wang, G.; Richter, R.; Rodahl, M.; Kasemo, B. QCM-D and reflectometry instrument: Applications to supported lipid structures and their biomolecular interactions. *Anal. Chem.* **2009**, *81* (1), 349–361.
- (7) Hamai, C.; Yang, T. L.; Kataoka, S.; Cremer, P. S.; Musser, S. M. Effect of average phospholipid curvature on supported bilayer formation on glass by vesicle fusion. *Biophys. J.* **2006**, *90* (4), 1241–1248.
- (8) Hamai, C.; Cremer, P. S.; Musser, S. M. Single giant vesicle rupture events reveal multiple mechanisms of glass-supported bilayer formation. *Biophys. J.* **2007**, *92* (6), 1988–99.
- (9) Richter, R. P.; Berat, R.; Brisson, A. R. Formation of solid-supported lipid bilayers: An integrated view. *Langmuir* **2006**, *22* (8), 3497–3505.

(10) Radler, J.; Strey, H.; Sackmann, E. Phenomenology and kinetics of lipid bilayer spreading on hydrophilic surfaces. *Langmuir* **1995**, *11* (11), 4539–4548.

(11) Richter, R.; Mukhopadhyay, A.; Brisson, A. Pathways of lipid vesicle deposition on solid surfaces: A combined QCM-D and AFM study. *Biophys. J.* **2003**, *85* (5), 3035–3047.

(12) Richter, R. P.; Brisson, A. R. Following the formation of supported lipid bilayers on mica: A study combining AFM, QCM-D, and ellipsometry. *Biophys. J.* **2005**, *88* (5), 3422–3433.

(13) Brian, A. A.; McConnell, H. M. Allogeneic stimulation of cytotoxic T-cells by supported planar membranes. *Proc. Natl. Acad. Sci. U. S. A.* **1984**, *81* (19), 6159–6163.

(14) Sackmann, E. Supported membranes: Scientific and practical applications. *Science* **1996**, *271* (5245), 43–48.

(15) Keller, C. A.; Glasmaster, K.; Zhdanov, V. P.; Kasemo, B. Formation of supported membranes from vesicles. *Phys. Rev. Lett.* **2000**, *84* (23), 5443–5446.

(16) Reviakine, I.; Rossetti, F. F.; Morozov, A. N.; Textor, M. Investigating the properties of supported vesicular layers on titanium dioxide by quartz crystal microbalance with dissipation measurements. *J. Chem. Phys.* **2005**, *122* (20), 204711–204718.

(17) Seifert, U. Configurations of fluid membranes and vesicles. *Adv. Phys.* **1997**, *46* (1), 13–137.

(18) Cho, N. J.; Jackman, J. A.; Liu, M.; Frank, C. W. pH-driven assembly of various supported lipid platforms: A comparative study on silicon oxide and titanium oxide. *Langmuir* **2011**, *27* (7), 3739–3748.

(19) Boudard, S.; Seantier, B.; Breffa, C.; Decher, G.; Felix, O. Controlling the pathway of formation of supported lipid bilayers of DMPC by varying the sodium chloride concentration. *Thin Solid Films* **2006**, *495* (1–2), 246–251.

(20) Seantier, B.; Breffa, C.; Felix, O.; Decher, G. Dissipation-enhanced quartz crystal microbalance studies on the experimental parameters controlling the formation of supported lipid bilayers. *J. Phys. Chem. B* **2005**, *109* (46), 21755–21765.

(21) Seantier, B.; Kasemo, B. Influence of mono- and divalent ions on the formation of supported phospholipid bilayers via vesicle adsorption. *Langmuir* **2009**, *25* (10), 5767–5772.

(22) Seifert, U.; Lipowsky, R. Adhesion of vesicles. *Phys. Rev. A* **1990**, *42* (8), 4768–4771.

(23) Mornet, S.; Lambert, O.; Duguet, E.; Brisson, A. The formation of supported lipid bilayers on silica nanoparticles revealed by cryoelectron microscopy. *Nano Lett.* **2005**, *5* (2), 281–285.

(24) Reviakine, I.; Gallego, M.; Johannsmann, D.; Tellechea, E. Adsorbed liposome deformation studied with quartz crystal microbalance. *J. Chem. Phys.* **2012**, *136* (8), 084702–084705.

(25) van den Bogaart, G.; Mika, J. T.; Krasnikov, V.; Poolman, B. The lipid dependence of melittin action investigated by dual-color fluorescence burst analysis. *Biophys. J.* **2007**, *93* (1), 154–163.

(26) Haberman, E. Bee wasp venoms. *Science* **1972**, *177* (4046), 314.

(27) Cohen, B. E.; Bangham, A. D. Diffusion of small non-electrolytes across liposome membranes. *Nature* **1972**, *236* (5343), 173–4.

(28) Peterlin, P.; Arrigler, V. Electroformation in a flow chamber with solution exchange as a means of preparation of flaccid giant vesicles. *Colloids Surf., B* **2008**, *64* (1), 77–87.

(29) Branden, M.; Tabaei, S. R.; Fischer, G.; Neutze, R.; Hook, F. Refractive-index-based screening of membrane-protein-mediated transfer across biological membranes. *Biophys. J.* **2010**, *99* (1), 124–133.

(30) Brochard-Wyart, F.; de Gennes, P. G.; Sandre, O. Transient pores in stretched vesicles: role of leak-out. *Physica A* **2000**, *278* (1–2), 32–51.

(31) Wacklin, H. P. Composition and asymmetry in supported membranes formed by vesicle fusion. *Langmuir* **2011**, *27* (12), 7698–7707.

(32) Anderson, T. H.; Min, Y. J.; Weirich, K. L.; Zeng, H. B.; Fygenon, D.; Israelachvili, J. N. Formation of supported bilayers on silica substrates. *Langmuir* **2009**, *25* (12), 6997–7005.

- (33) Huang, C. H. Studies on phosphatidylcholine vesicles. Formation and physical characteristics. *Biochemistry* **1969**, *8* (1), 344–&..
- (34) Tellechea, E.; Johannsmann, D.; Steinmetz, N. F.; Richter, R. P.; Reviakine, I. Model-independent analysis of QCM data on colloidal particle adsorption. *Langmuir* **2009**, *25* (9), 5177–5184.
- (35) Müller, D. J.; Amrein, M.; Engel, A. Adsorption of biological molecules to a solid support for scanning probe microscopy. *J. Struct. Biol.* **1997**, *119* (2), 172–188.
- (36) Reviakine, I.; Johannsmann, D.; Richter, R. P. Hearing what you can't see and visualizing what you hear: interpreting quartz crystal microbalance data from solvated interfaces. *Anal. Chem.* **2011**, *83* (23), 8838–8848.
- (37) McDaniel, R. V.; McIntosh, T. J.; Simon, S. A. Non-electrolyte substitution for water in phosphatidylcholine bilayers. *Biochim. Biophys. Acta* **1983**, *731* (1), 97–108.
- (38) Boggs, J. M.; Rangaraj, G. Phase transitions and fatty acid spin label behavior in interdigitated lipid phases induced by glycerol and polymyxin. *Biochim. Biophys. Acta* **1985**, *816* (2), 221–33.
- (39) Johansson, L. B. A.; Kalman, B.; Wikander, G.; Fransson, A.; Fontell, K.; Bergenstahl, B.; Lindblom, G. Phase-equilibria and formation of vesicles of dioleoylphosphatidylcholine in glycerol water mixtures. *Biochim. Biophys. Acta* **1993**, *1149* (2), 285–291.
- (40) Hermens, W. T.; Benes, M.; Richter, R.; Speijer, H. Effects of flow on solute exchange between fluids and supported biosurfaces. *Biotechnol. Appl. Biochem.* **2004**, *39*, 277–284.
- (41) Rawicz, W.; Olbrich, K. C.; McIntosh, T.; Needham, D.; Evans, E. Effect of chain length and unsaturation on elasticity of lipid bilayers. *Biophys. J.* **2000**, *79* (1), 328–339.
- (42) Johnson, J. M.; Ha, T.; Chu, S.; Boxer, S. G. Early steps of supported bilayer formation probed by single vesicle fluorescence assays. *Biophys. J.* **2002**, *83* (6), 3371–3379.
- (43) Schonherr, H.; Johnson, J. M.; Lenz, P.; Frank, C. W.; Boxer, S. G. Vesicle adsorption and lipid bilayer formation on glass studied by atomic force microscopy. *Langmuir* **2004**, *20* (26), 11600–11606.
- (44) Lenz, P.; Johnson, J. M.; Chan, Y. H. M.; Boxer, S. G. Tension-induced pore formation and leakage in adhering vesicles. *Europhys. Lett.* **2006**, *75* (4), 659–665.
- (45) Mui, B. L. S.; Cullis, P. R.; Evans, E. A.; Madden, T. D. Osmotic properties of large unilamellar vesicles prepared by extrusion. *Biophys. J.* **1993**, *64* (2), 443–453.
- (46) Burgess, J. *Metal Ions in Solution*; Ellis Horwood: New York, 1978.